analytical chemistry

pubs.acs.org/ac Article

Electrochemical DNA Scaffold-Based Sensing Platform for Multiple Modes of Protein Assay and a Keypad Lock System

Li Wang, Xu Wang, Zhiqiang Chen, and Shufeng Liu*

Cite This: *Anal. Chem.* 2022, 94, 8317−8326 Read Online

ACCESS | Metrics & More | Article Recommendations | Supporting Information

ABSTRACT: Development of a flexible, easy-to-use, and well-controllable DNA-based sensing platform would provide enormous opportunities to boost molecular diagnosis and signal transduction or information processing. Herein, a duplex DNA scaffold containing a bulge was deployed for the fabrication of a simple and general DNA-based electrochemical sensing platform. It could be harnessed for different signal output behaviors (one signal-off and two signal-on modes) toward a single-step analysis of the target protein. The detection limit toward the target protein could reach about 0.1 nM. Also, it could be used as a streamlined electrochemical workflow for the successive monitoring of protein binding. Furthermore, such an electrochemical sensing platform could be explored for the operation of the concatenated AND logic gates as a molecular keypad lock system. The current sensing platform based on only one duplex DNA scaffold presented features such as simple biosensor design and fabrication, flexible operation for different signal outputs, sensitive and selective protein detection, and expandable logic operation. It thus would pave a broad road toward the development of high-performance biosensors or logic devices to be applied for molecular diagnosis or computing.

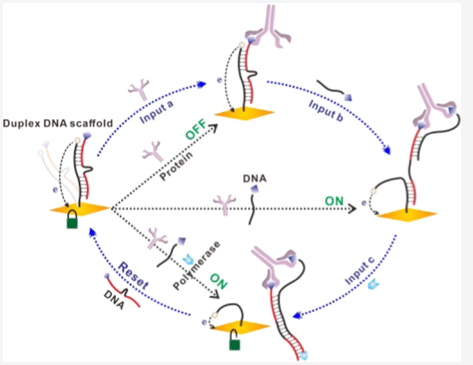

INTRODUCTION

Sensitive and accurate protein analysis using an easy-to-use sensing platform is critical for disease diagnosis, monitoring, and therapy.[1−3] Typical protein analysis methods such as sandwich enzyme-linked immunosorbent assays (ELISA) and western blotting require multistep, time-consuming procedures and sophisticated instrumentations that would limit their wide applications in routine clinical diagnosis.[4−6] To accommodate point-of-care applications, many research efforts were devoted to develop sensitive and specific biosensors that simultaneously possessed the features of facile operation, rapid response, and low operating and equipment cost.[7−9]

Over the past decades, a number of DNA-based sensing platforms had been well exploited for protein analysis.[10,11] Electrochemical biosensors were especially suited for point-of-care applications.[12−15] Among them, electrochemical DNA switch-based biosensors showed the single-step and reagentless features and had been validated for target detection in complex clinical samples.[16−18] The mechanism of target binding-induced conformational change in the recognition element (engineered nucleic acid probe or DNA scaffold) was dedicated to signal generation. However, it needed a large-scale conformational change in the receptor that was only suitable for some specific targets. For more generality, a similar electrochemical DNA switch with a stem-loop structure was designed for the quantitative detection of antibodies.[19] However, the DNA switch required multiple conjugations on the respective strands (two copies of an antigen or epitope and the signal reporter elements). Also, the signal output of the DNA switch was strongly affected by the size of proteins. In this context, research efforts were also steered to some other routes for DNA-based protein analysis that did not rely on the structure switching mechanism.[20] For example, the rigid double-stranded nucleic acid scaffold, with the labeled redox molecule as a signal reporter and the small-molecule moiety as a recognition element, was proposed for single-step protein detection.[21,22] The steric hindrance effect was also explored to develop single-step DNA-based biosensors in which antibody binding with the redox-active signaling strand altered its hybridization kinetics with a capture DNA.[23,24] Unfortunately, these platforms could only operate in a signal-off fashion, limiting the signal gain of the sensor. To improve the signal gain, the proximity-based nucleic acid hybridization strategy became popular for single-step and signal-on protein analysis.[25−30] It was also confronted by the complex thermodynamic optimization of the involved multiple DNA sequences, which was responsible for the cooperative recognition effect. Thus, the design of a more flexible, versatile, and easy-to-use sensing platform for highly accurate protein assay was still desirable.

Received: February 17, 2022
Accepted: May 18, 2022
Published: June 1, 2022

https://doi.org/10.1021/acs.analchem.2c00800
Anal. Chem. 2022, 94, 8317−8326

Based on the above-mentioned arguments, herein, a duplex DNA scaffold probe was initially designed to facilitate a simple, flexible, and universal DNA-based sensing platform. The duplex DNA scaffold was labeled with a ferrocene as a redox reporter and a protein recognition element, which was located at the distal termini at the respective DNA strands when the duplex DNA scaffold was immobilized on the electrode. The duplex DNA scaffold was also designed with a bulge region at one of the DNA strands to endow the flexible operation for DNA strand displacement and extension. Such a fabricated electrochemical sensing platform using only one duplex DNA scaffold could flexibly harness signal response behaviors and detection performance toward the target protein. This included a direct, single-step, and reagent-less protein analysis based on a protein binding-induced signal-off mechanism. Coupling with a recognition element-functionalized DNA for strand displacement or together with a polymerase for DNA extension presented two single-step and signal-on response mechanisms for protein detection with the sequentially improved signal gains. It could also enable a streamlined workflow for successive and multilevel signal monitoring of protein binding by stepwise introduction of protein, functionalized DNA, and DNA polymerase. Inspired by this streamlined workflow principle, a new electrochemical molecular keypad lock system was further proposed. Rather than merely molecular recognition and quantitation, the molecular keypad lock could be operated for information protection as a molecular security data processor and has received increasing attention.[31−33] The current sensing platform based on only one duplex DNA scaffold presented the advantageous features of simplicity in biosensor fabrication, flexibility in biosensor operation, different signal output behaviors for sensitive protein analysis, and expandable logic operation.

EXPERIMENTAL SECTION

Reagents and Chemicals. 6-Mercapto-1-hexanol (MCH), 4-(2-hydroxyethyl)piperazine-1 ethanesulfonic acid sodium salt (HEPES), hexaammineruthenium(III) chloride (RuHex), streptavidin (STA), and sheep polyclonal anti-digoxigenin antibody (anti-dig antibody) were obtained from Sigma-Aldrich (St. Louis, MO). Bst DNA polymerase (Large Fragment) was purchased from New England Biolabs Inc. (Ipswich, MA). The deoxyribonucleoside 5′-triphosphate (dNTP) mixture and tris(2-carboxyethyl)phosphine hydrochloride (TCEP) were purchased from Sangon Biotech Co., Ltd. (Shanghai, China). The mouse monoclonal anti-5-methylcytosine antibody (anti-5-mC) was purchased from Active Motif (San Diego, CA). The monoclonal antibody to prostate-specific antigen (Anti-PSA) was purchased from Shanghai Linc-Bio Science Co., Ltd. (Shanghai, China). Serum was purchased from Sangon Biotech. Co., Ltd. (Shanghai, China). The HPLC-purified ferrocene-labeled DNA sequences were synthesized by Nanjing Genscript Biotechnology Co., Ltd. (Nanjing, China). All other DNA sequences were HPLC-purified and synthesized by Sangon Biotech. Co., Ltd. (Shanghai, China). The DNA sequences are shown in Tables S1−S4.

Preparation of the Duplex DNA Scaffold-Modified Electrode. Gold electrodes were pretreated with the first immersion in a fresh piranha solution (volume ratio for H_2SO_4 and H_2O_2 of 3:1) for 10 min to remove any possible organic pollutants. After that, the electrodes were polished with alumina oxide slurries (0.05 μm), followed by sonication in ethanol and water each for 5 min. Finally, the electrodes were electrochemically scanned in 0.5 M H_2SO_4 solution between −0.2 and +1.5 V with 100 mV/s till a stable cyclic voltammogram curve was reached. The effective working area for bare gold electrodes could be calculated to be about 0.027 cm^2 according to the Randles−Sevcik equation (Figure S1).[34] To serve for reproducible results, the bare electrodes with the approximate working area were always used.

The duplex DNA scaffold probe was obtained by annealing DNA1 and DNA2 with a molar ratio of 1:1.2 in 1 M $NaClO_4$ containing 1 mM TCEP. The mixture was first heated to 90 °C and then slowly cooled to room temperature. Then, the duplex DNA scaffold probe was ready for immobilization at the electrode surface.

The duplex DNA scaffold probe-modified electrodes were prepared by incubating the electrodes in a thiolated duplex DNA scaffold with appropriate concentrations (50, 200, and 1000 nM) for 2 h at room temperature, followed by post-treatment with 0.1 M MCH in 1 M $NaClO_4$ for 1 h. Then, the electrodes were rinsed and stored in 10 mM HEPES (pH 8.0, 50 mM $NaClO_4$) before use. The use of $NaClO_4$ could avoid the instability of ferrocenium (the oxidized form of ferrocene).[35,36]

Different Assay Modes for the Protein. The duplex DNA scaffold-modified electrode was used as the unified sensing interface for different assay modes (I−III) toward protein recognition. For reagent-less anti-dig antibody analysis (assay mode I), the modified electrodes were incubated in 10 mM HEPES (pH 8.0, 50 mM $NaClO_4$) containing various concentrations of anti-dig antibody for 40 min at 37 °C. For assay mode II based on the proximity recognition-induced strand displacement strategy, the modified electrodes were incubated in 10 mM HEPES (pH 8.0, 50 mM $NaClO_4$) containing 100 nM DNA3 and various concentrations of anti-dig antibody for 40 min at 37 °C. For assay mode III based on the proximity recognition and DNA polymerization-induced strand displacement strategy, the modified electrodes were incubated in 10 mM HEPES (pH 8.0, 50 mM $NaClO_4$) containing 100 nM DNA3, 8 U Bst DNA polymerase, 200 μM dNTPs, and various concentrations of anti-dig antibody for 40 min at 37 °C. The above-mentioned different assay modes were also applied for streptavidin analysis, but the recognition element conjugated onto the duplex DNA scaffold probe was replaced with biotin.

Consecutive and Multilevel Monitoring of Protein. The duplex DNA scaffold-modified electrodes were first incubated in 10 mM HEPES (pH 8.0, 50 mM $NaClO_4$) containing various concentrations of anti-dig antibody for 30 min at 37 °C (step 1). After rinsing with 10 mM HEPES (pH 8.0, 50 mM $NaClO_4$), the protein-recognized electrodes were incubated with 10 mM HEPES (pH 8.0, 50 mM $NaClO_4$) containing 100 nM DNA3 for 30 min at 37 °C (step 2). After rinsing again with 10 mM HEPES (pH 8.0, 50 mM $NaClO_4$), the protein- and DNA3-recognized electrodes were incubated with 10 mM HEPES (pH 8.0, 50 mM $NaClO_4$) containing 8 U Bst DNA polymerase and 200 μM dNTPs for 30 min at 37 °C (step 3).

Operation of the Concatenated AND Logic Gates as a Keypad Lock System. The duplex DNA scaffold-modified electrode is the initial state of the keypad lock. The operation for the input abc was based on the procedures given below. The duplex DNA-modified electrode was incubated in 10 mM HEPES (pH 8.0, 50 mM $NaClO_4$) containing 100 nM anti-dig

https://doi.org/10.1021/acs.analchem.2c00800
Anal. Chem. 2022, 94, 8317−8326

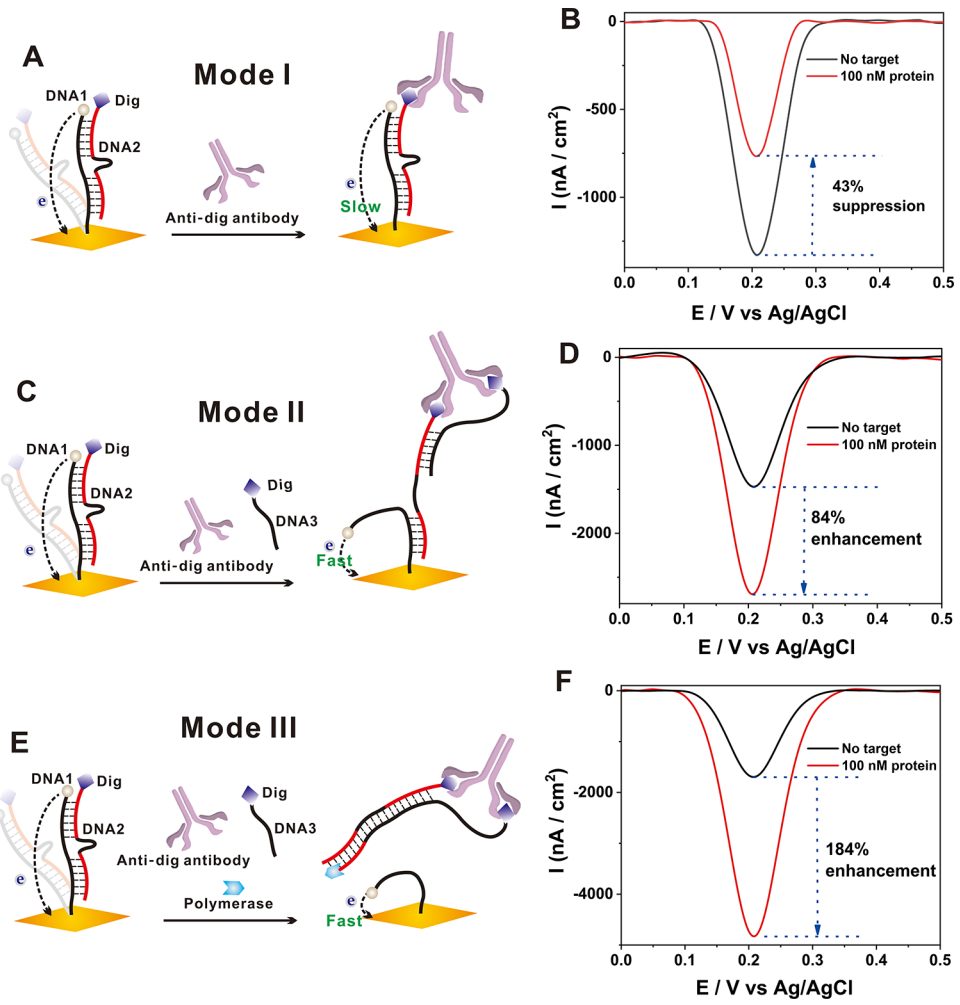

Figure 1. Schematic illustration of different assay modes (I–III) using only one duplex DNA scaffold interface (A, C, E). Electrochemical responses toward 0 and 100 nM anti-dig antibody (B, D, F). Three sensing modes include reagent-less and signal-off mode I (A, B), proximity-based strand displacement mode II (C, D), and proximity and DNA polymerase-guided strand displacement mode III (E, F).

antibody (input a) for 30 min at 37 °C to obtain the protein-bound electrode. Then, the protein-bound electrode was incubated in 10 mM HEPES (pH 8.0, 50 mM $NaClO_4$) containing 100 nM DNA3 (input b) for 30 min at 37 °C to obtain the protein- and DNA3-recognized electrode. The protein- and DNA3-recognized electrode was then immersed in 10 mM HEPES (pH 8.0, 50 mM $NaClO_4$) containing 8 U Bst DNA polymerase and 200 μM dNTPs (input c) for 30 min at 37 °C to obtain the DNA1-released electrode. After each input, the electrodes were rinsed with 10 mM HEPES (pH 8.0, 50 mM $NaClO_4$). The operation for the keypad lock in other different input permutations (acb, bac, bca, cab, and cba) was based on the same way as mentioned above. After execution of the keypad lock, the keypad lock was reset by incubating in input b and c in sequence according to the above-mentioned procedure, followed by hybridization of the obtained electrode with 200 nM DNA2 for 1 h at 37 °C.

Electrochemical Measurement. Electrochemical measurements were performed with a CHI 660E electrochemical workstation (CH Instruments, Shanghai, China). The SWV characterization was carried out in 10 mM HEPES (pH 8.0, 50 mM $NaClO_4$) by scanning the potential from 0 to 0.5 V with an increase of 4 mV and amplitude of 25 mV. Electrochemical impedance spectroscopy (EIS) and cyclic voltammetry (CV) characterizations toward the stepwise fabrication of the modified electrode were conducted in 5 mM $[Fe(CN)_6]^{3-/4-}$ of 10 mM PBS buffer (pH 7.4, 1 M KCl). The applied frequency for EIS was in the range from 0.1 Hz to 100 kHz. The scan rates for CV were 100 mV/s. The chronocoulometry characterizations toward the assembly density of the duplex DNA probe were performed in 10 mM Tris-HCl (pH 7.4) containing 50 μM RuHex with an initial potential of 0.5 V, a final potential of 0 V, and a pulse width of 0.25 s.

RESULTS AND DISCUSSION

Duplex DNA Scaffold-Based Sensing Platform for Single-Step and Multiple Signal Response Behaviors toward the Protein. The sensing interface was constructed easily by immobilizing a duplex DNA scaffold probe, which was annealed by two single-stranded DNA (DNA1 and DNA2), on the electrode (Figure 1). The DNA1 was modified with a mercaptol group at the 3′-terminus for anchoring on the electrode and a ferrocene group at the 5′-terminus as a redox reporter. The DNA2 was modified with a protein recognition element at the 3′-terminus. The formed duplex DNA probe contained a bulge (unhybridized region) at DNA2. The duplex DNA scaffold probe was immobilized onto the electrode by a flexible linker that could allow the redox reporter (ferrocene)

https://doi.org/10.1021/acs.analchem.2c00800
Anal. Chem. 2022, 94, 8317−8326

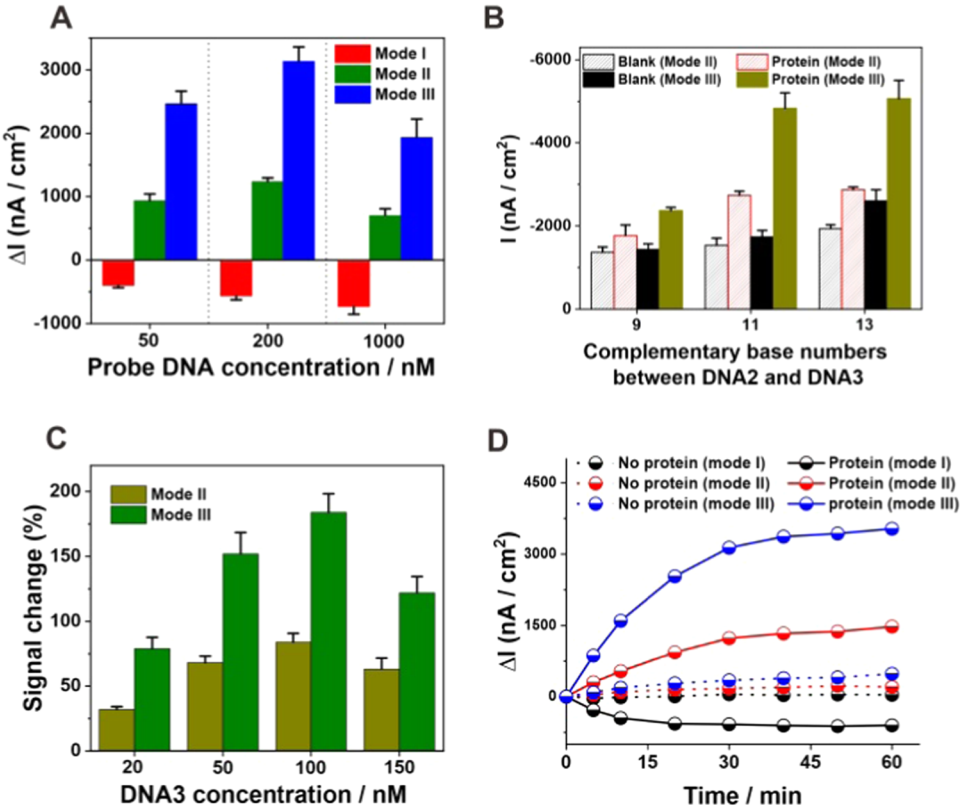

Figure 2. (A) Current changes toward 100 nM anti-dig antibody according to three sensing modes at different probe DNA concentrations (50, 200, and 1000 nM). (B) Optimization of complementary base numbers between DNA2 and DNA3. (C) Optimization of DNA3 concentration. (D) Current change plots at different assay modes with the reaction time.

to approach the electrode for electron transfer. At the initial immobilization status of the duplex DNA scaffold, the redox reporter and the protein recognition element were adjacent and located at the distal termini from the electrode. Such a fabricated sensing interface could be simultaneously used for single-step protein analysis according to different signal response modes including mode I (Figure 1A), mode II (Figure 1C), and mode III (Figure 1E). It should be noted that the current duplex DNA scaffold-based sensing platform would be more suitable for the detection of the bivalent or multivalent proteins. Herein, the anti-dig antibody was first chosen as a model protein and the digoxigenin (abbreviated as dig) was chosen as the recognition element. For assay mode I, protein binding limited the diffusion of the tethered redox reporter toward the electrode surface for the suppressed signal response.[20−22] Thus, the assay mode I offered the opportunity for direct, single-step, and reagent-less analysis of the target protein. It could be seen from Figure 1B that the electrochemical response upon protein binding was evidently attenuated. The mode II was based on a proximity recognition-induced strand displacement strategy by introducing an additional dig-labeled DNA (DNA3). The DNA3 was designed to be complementary with the partial sequence of DNA2. The simultaneous recognition of the anti-dig antibody with the two dig elements conjugated onto DNA2 and DNA3 brought about their proximity hybridization owing to the increased local concentrations,[26−28] inducing the partial sequence at the 5′-terminus of DNA1 to be displaced and dissociated from DNA2. This promoted the redox reporter to approach the electrode for the increased electron transfer. Thus, a single-step and signal-on electrochemical assay mode for the protein was obtained. The corresponding characterizations using or not using the anti-dig antibody are shown in Figure 1D. Only a slightly increased background response in the absence of the anti-dig antibody suggested that DNA3 was very difficult to hybridize with DNA2 owing to the stronger hybridization stability between DNA1 and DNA2. Upon addition of the anti-dig antibody, an evidently enhanced electrochemical response was evoked. Furthermore, the assay mode III could be realized with the concurrent introduction of DNA polymerase on the basis of mode II (Figure 1E). In this case, after protein binding-induced proximity recognition between DNA2 and DNA3, the 3′-terminus of DNA3 would be further elongated by DNA polymerase, ultimately inducing the DNA1 to be completely dissociated from DNA2. The remaining DNA1 on the electrode presented a flexible single-stranded structure, making the redox reporter approach the electrode surface more easily for the further enhanced electron transfer. Again, a relatively low background response by DNA3 and polymerase and a more significant signal response toward the same concentration of protein were observed (Figure 1F). The slightly increased background response for mode II and III relative with mode I might be induced by the minute amount of direct hybridization between DNA3 and DNA2 to dissociate the partial or full sequence of DNA1.

A series of control experiments were conducted to support the above-mentioned principle (Figures S2 and S3). Using a duplex DNA scaffold with no dig label as a substitute, the anti-dig antibody induced no evident signal changes in modes I−III. Also, using DNA3 with no dig label as a substitute in modes II and III, only current suppression induced by protein binding but no enhanced current response by DNA3-based

https://doi.org/10.1021/acs.analchem.2c00800
Anal. Chem. 2022, 94, 8317−8326

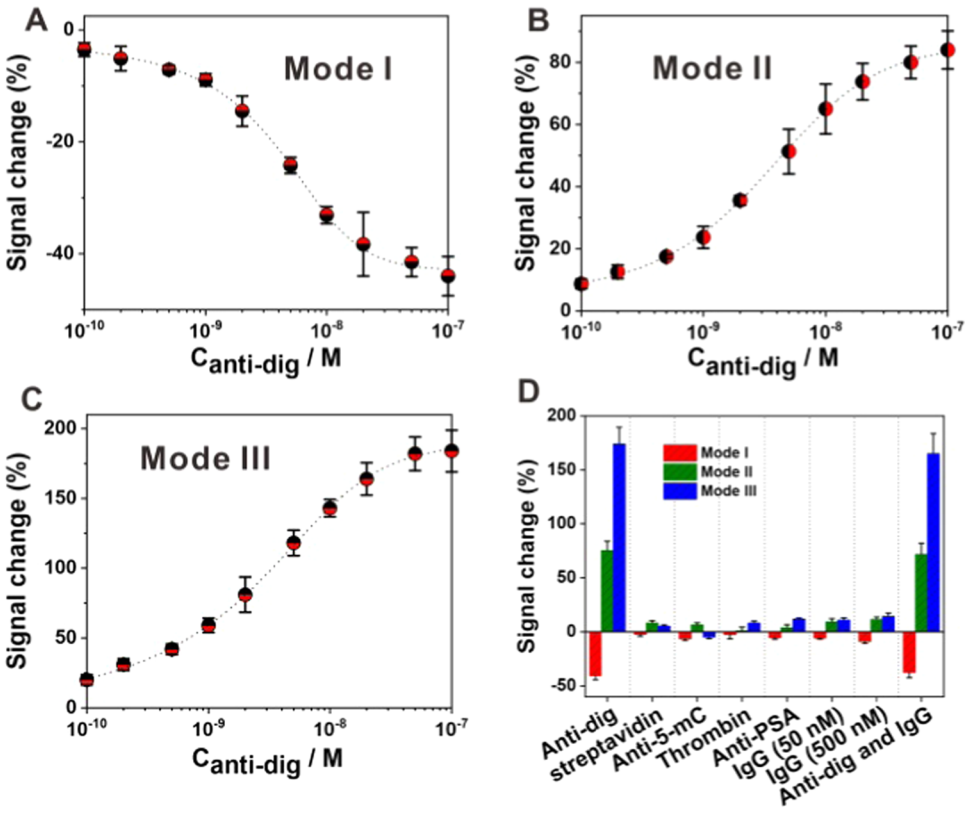

Figure 3. Assay performance toward different concentrations of the anti-dig antibody based on three different assay modes: I (A); II (B), and III (C). (D) Detection selectivity toward different proteins including the anti-dig antibody (50 nM), streptavidin (50 nM), anti-5-methylcytosine antibody (anti-5-mC, 50 nM), thrombin (50 nM), antibody for prostate-specific antigen (anti-PSA, 50 nM), human IgG (50 and 500 nM), and the mixture of anti-dig (50 nM) and IgG (500 nM).

strand displacement or polymerization extension occurred (Figure S2). We also designed another DNA3 with a prolonged 4-base tail at the 3′-terminus, and these extended bases were not complementary with DNA2. In this case, the current response by mode III was only comparable with that by mode II, indicating that the recognized DNA3 could be not elongated by DNA polymerase owing to the overhung four bases at the 3′-termini (Figure S3). The introduction of a bulge loop at DNA2 was critical for the operation of multiple assay modes, especially for modes II and III. As to this point, four different duplex DNA scaffold probes (P1−P4) were designed for comparison (Figure S4). The P1 structure was used throughout the text. P2 contained no bulge loop, and the bulge loop for P3 was located at DNA1. P4 possessed the bulge loops at both DNA1 and DNA2. The complementary base numbers between DNA3 and DNA2 for these probes were equal for a rational comparison. As for the P2 and P3 structures, the DNA2 sequence was completely caged by DNA1, and the hybridization recognition between DNA3 and DNA2 was difficult even upon protein binding. They could not effectively work for protein assay in modes II and III. The P4 structure also showed the detection feasibility for protein according to different assay modes. However, it presented a relatively flexible DNA skeleton, and the signal gains for all the assay modes were inferior to those of the P1 structure. These control experiments could support the signal origin of multiple assay modes. The fluorescence characterization for the current duplex DNA scaffold-based sensing platform was also conducted (see Figure S5 and the corresponding experimental details in the Supporting Information). Only in the coexistence of the anti-dig antibody, DNA3, and polymerase, DNA1 could be completely dissociated from DNA2 for distinct fluorescence recovery, further verifying the working principle of the current duplex DNA scaffold-based sensing platform.

Optimization of Assay Conditions. The corresponding experimental conditions for the current multiple assay modes were optimized. First, three different immobilization concentrations (50, 200, and 1000 nM) of the duplex DNA scaffold were studied, and an intermediate concentration (200 nM) was better suited for the signal gains toward the protein, especially in the case of assay modes II and III (Figure 2A). At a higher concentration of 1000 nM, the assay mode I demonstrated a more evident signal suppression, which might be explained that a higher packing density of the duplex DNA probe magnified the steric hindrance effect after protein binding to limit the approaching of the redox reporter toward the electrode. The assembly densities of the duplex DNA scaffold onto the electrode were estimated according to the reported method,[37] and they were about 1.6×10^{11}, 5.6×10^{11}, and 3.2×10^{12} molecules/cm^2 at the immobilization concentration of 50, 200, and 1000 nM, respectively. The average occupied area for each duplex DNA molecule on the electrode was calculated as 625, 178.6, and 31.3 nm^2 based on the reciprocal value of the assembly density. Then, the average distances between probes were further calculated as about 28, 15, and 6.3 nm between each duplex DNA probe. Considered with the size of the antibody (about 12 nm), such an average distance (15 nm for 200 nM duplex DNA probe) was beneficial to avoid the undesired binding of the protein with two adjacent recognition elements onto the electrode, which

https://doi.org/10.1021/acs.analchem.2c00800
Anal. Chem. 2022, 94, 8317−8326

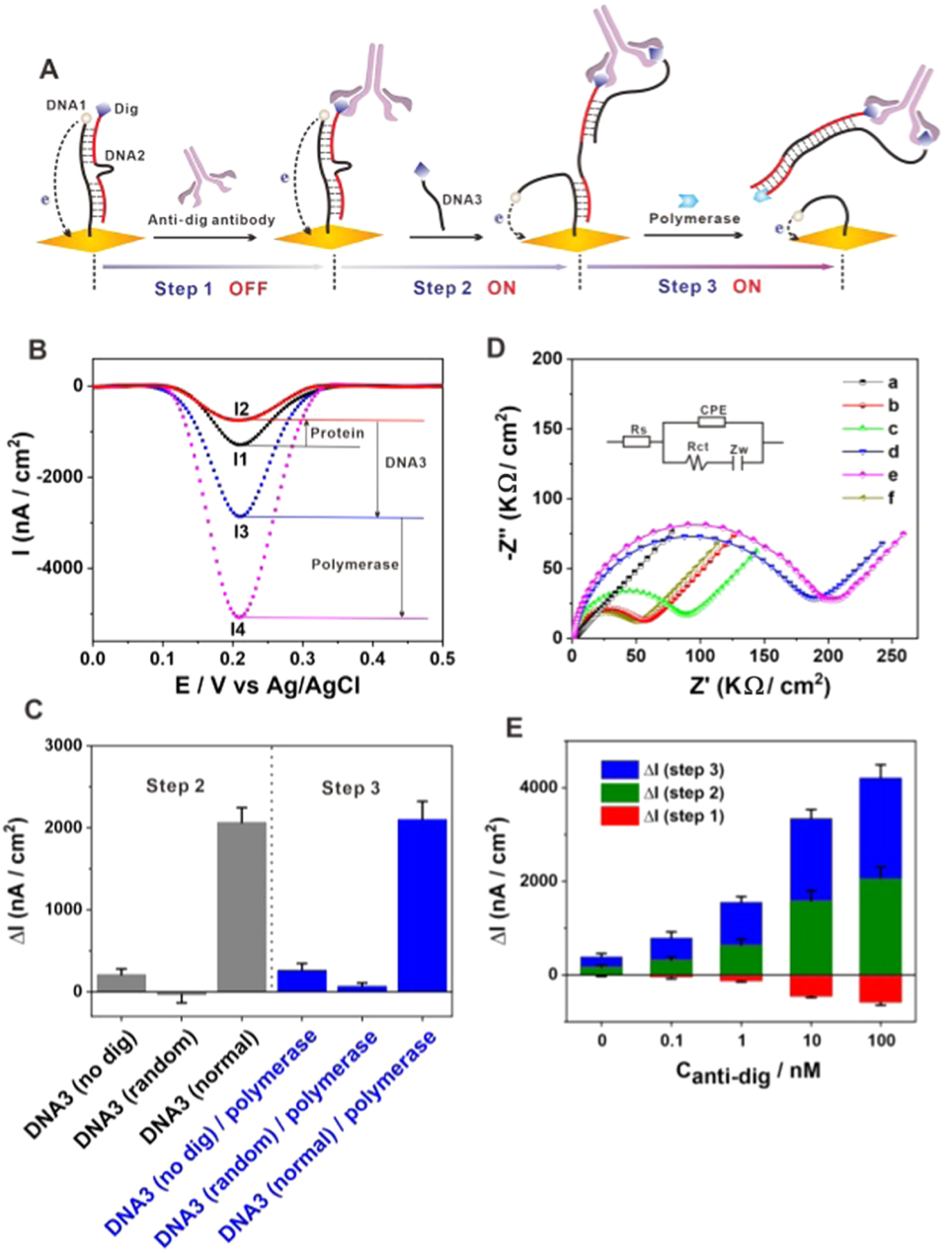

Figure 4. (A) Schematic illustration of the streamlined electrochemical workflow for successive monitoring of protein binding. (B) Electrochemical responses for the initial duplex DNA scaffold-modified electrode (I1) and after the sequential operation by protein binding (I2) and DNA3 incubation (I3) and addition of DNA polymerase (I4), respectively. (C) Current changes for step 2 (ΔI = I3 − I2) and step 3 (ΔI = I4 − I3) under different control conditions using DNA3 with no dig label or with a random base sequence. (D) EIS spectra for the differently fabricated electrodes: gold electrode (curve a), after duplex DNA scaffold modification (curve b), MCH assembly (curve c), protein binding (curve d), DNA3 introduction (curve e), and DNA extension by polymerase (curve f). (E) Current changes for each step (step 1−3) at different concentrations of anti-dig antibody.

would be detrimental to the signal responses of assay modes II and III. It might be the reason for the signal response sacrifice in assay modes II and III at a higher immobilization concentration of 1000 nM. The complementary base numbers between DNA3 and DNA2 were optimized based on the signal responses of assay modes II and III. The hybridized base number of 11 was best for the signal response toward the protein (Figure 2B). The small base number (9) between them weakened the protein binding-induced hybridization recognition for the low signal response, and the large base number (13) between them made the increased background level. The concentration of DNA3 also affected the signal response of assay modes II and III toward the protein. The maximum signal gain toward the protein was obtained at 100 nM of DNA3 for both assay modes II and III (Figure 2C). The time dependence of protein binding at different assay modes was studied (Figure 2D). The protein recognition could be almost accomplished within 30 min for all the assay modes, presenting the rapid protein analysis ability.

Detection Performance of Proteins by Three Different Assay Modes. To explore the detection capability of different assay modes for the protein, the response curves

https://doi.org/10.1021/acs.analchem.2c00800
Anal. Chem. 2022, 94, 8317−8326

versus different concentrations of the protein were studied and are shown in Figure 3. The typical SWV responses at different concentrations of the anti-dig antibody for different assay modes (I−III) are shown in Figure S6. In mode I, the signal suppression efficiency enlarged with the increasing anti-dig antibody concentrations in the range of 10^{-10}−10^{-7} M (Figure 3A). An evident signal suppression efficiency of about 15% could be observed at an anti-dig antibody concentration of 2 nM. In mode II, the signal enhancement efficiency upgraded continuously with the increasing anti-dig antibody concentrations, indicating also its protein concentration-dependent response behavior (Figure 3B). At 0.2 nM anti-dig antibody, a signal increase efficiency of about 13% could be observed, suggesting its better detection sensitivity. The detection sensitivity for the anti-dig antibody could be further upgraded by mode III (Figure 3C). The signal enhancement efficiency of about 20% could be easily achieved at a low concentration of anti-dig antibody of 0.1 nM. The detection sensitivity for the current sensing platform was comparable with or superior to that of many reported methods (Table S5). However, further optimization was still necessary to match the sensitivity of some DNA amplification-based methods or ELISA. The relative standard deviations toward different concentrations of proteins by the current DNA scaffold-based sensing platform could basically fall within the value range less than 15%, which compared favorably with the reported DNA-based electrochemical methods but was inferior to some optical methods. The relatively good detection reproducibility could be attributed to the dependence of the signal gain for protein binding upon current change but not current, which could avoid the influence from the variations in the electrode or sensing layer to a large extent. Also, the control for a basically consistent sensing interface and the efficient signal response only triggered by specific interactions would be beneficial for the detection reproducibility.

The detection selectivity toward the anti-dig antibody by the three assay modes was also checked (Figure 3D). All three assay modes displayed relatively good discrimination selectivity toward the anti-dig antibody even at a high concentration of nonspecific protein. The selectivity was at least in excess of 10^3 especially for modes II and III, which could be attributed to the high specificity of protein binding and double recognition event for signal output. The DNA-based sensing platform was considered to be relatively stable against degradation.[19,25] Then, the stability for the current duplex DNA scaffold-based sensing interface was examined. After storage at 4 °C for 10 days, the electrochemical responses toward protein were not evidently diminished (Figure S7A). In assay mode III, the sensing interface could be regenerated after the hybridization of the DNA1-released electrode with DNA2 (Figure S7B). The developed biosensor could also be feasible for protein detection in relatively complicated biological matrices such as serum. Comparable signal responses could be observed for different concentrations of anti-dig antibody spiked in buffer and diluted serum by different assay modes (Figure S8), suggesting that the signal response was relatively insensitive to sample variations except the concentration change of antibody.

By simply changing the recognition element conjugated onto the respective DNA, the sensing platform could be extended for detection toward other proteins. Herein, using biotin as a recognition element, the detection of streptavidin was studied. All three assay modes displayed the streptavidin concentration-dependent signal response behaviors (Figure S9). Also, the calibration curves for the signal responses versus streptavidin concentrations presented almost the same trend as that for the anti-dig antibody. Owing to a relatively small size of streptavidin relative with the anti-dig antibody, the signal suppression efficiency by protein binding in assay mode I was inferior to that of the anti-dig antibody. However, the assay mode I was still effective to indicate the protein binding. The recovery experiments of the current DNA scaffold-based sensing platform toward target proteins were performed based on assay mode III (Table S6). The recovery ratios of 88−115% with the relative standard deviations of 6.4−14.8% toward the spiked proteins suggested the relatively reliable protein analysis.

Streamlined Workflow for Consecutive Protein Monitoring. Herein, the assay modes II and III could be considered as the stepwise evolution of assay mode I via the introduction of recognition element-conjugated DNA3 or together with polymerase. Considered with the low background responses induced by DNA3 itself or its coexistence with polymerase, a streamlined electrochemical workflow was conceived for consecutive monitoring of protein binding. The principle for the sequential electrochemical monitoring of protein binding is schematically illustrated in Figure 4A.

The whole process included three successive monitoring steps that displayed various signal gains for each step. The above-discussed assay mode I could be considered as the first monitoring step (step 1). In this step, the signal suppression by protein binding gave the first-level confirmation of target information. After step 1, the bound protein (herein anti-dig antibody) remained at another unoccupied recognition site that could be further recognized by the dig-conjugated DNA3, inducing the release of the partial sequence of DNA1 from the caged status for a signal reversal. Since the DNA3 itself could only induce a negligible background response, the electrochemical signal enhancement during this step 2 was also highly correlated with the initial protein binding. This process corresponded to the second-level electrochemical monitoring of protein information. Then, the addition of DNA polymerase during step 3 induced the complete release of DNA1 for the further enhanced signal response. The signal enhancement in this step was also intrinsically aroused by the initial protein binding, displaying a third-level monitoring of the target protein. The results for the streamlined electrochemical monitoring of the protein binding are shown in Figure 4B. After protein binding during step 1, the current response was decreased from I1 to I2. Then, the current was reversely increased from I2 to I3 after addition of dig-DNA3 during step 2. The further introduction of DNA polymerase during step 3 made the current to be increased from I3 to I4. The current difference for each step could be attributed to the initial protein binding information. To confirm the signaling mechanism for step 2 and step 3, the DNA3 with no dig label or with a random base sequence was employed as a comparison. The distinctive current changes for step 2 and step 3 could be only obtained by the DNA3 with the dig label and correct base sequence (Figure 4C). This streamlined workflow was also stepwise characterized by the electrochemical impedance spectroscopy (EIS) method (Figure 4D). The charge transfer resistance (R_{ct}) increased stepwise after the assembly of the duplex DNA probe and MCH onto the electrode (curves a−c). After protein binding with the duplex DNA probe, a large increase of R_{ct} was observed owing to the bound protein, providing the steric hindrance for the diffusion

https://doi.org/10.1021/acs.analchem.2c00800
Anal. Chem. 2022, 94, 8317−8326

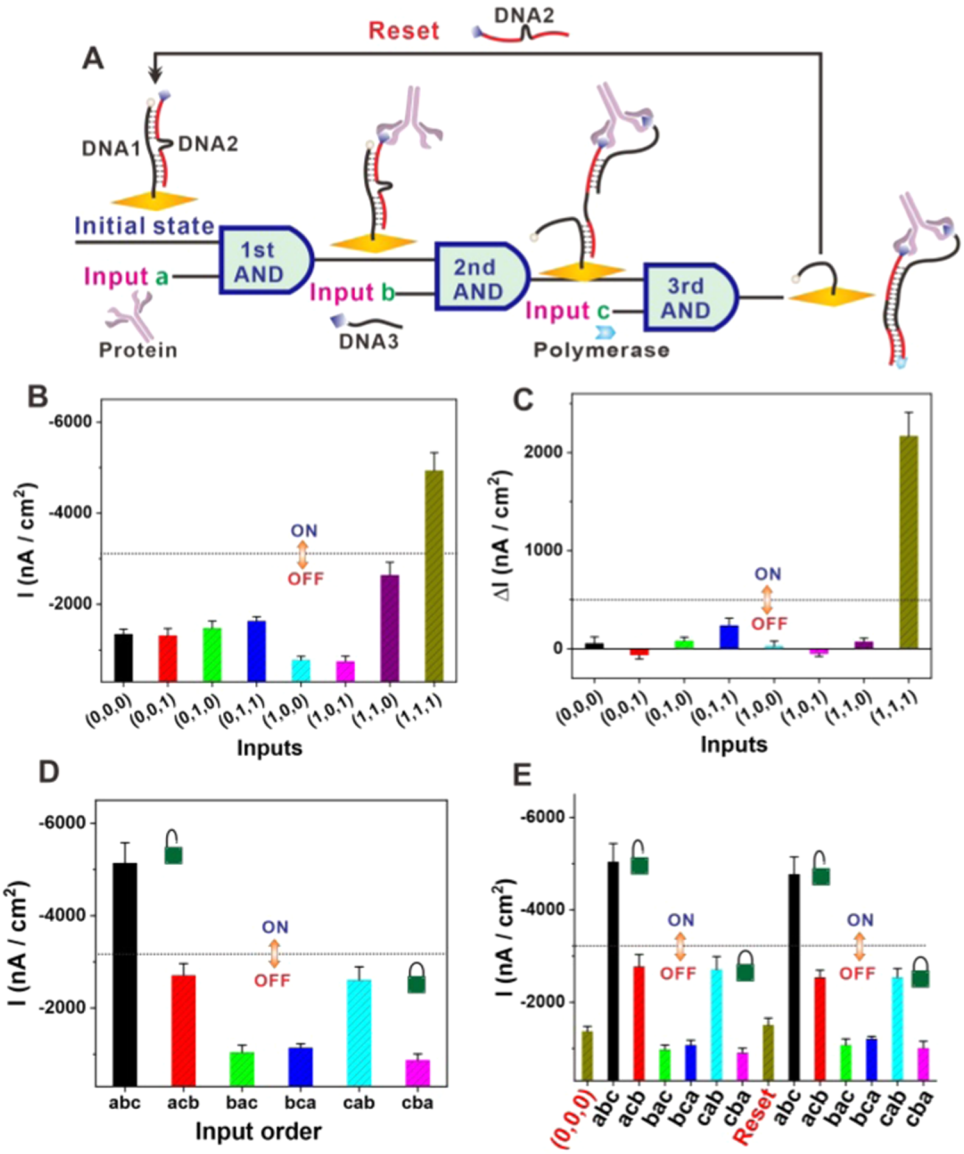

Figure 5. (A) Schematic illustration of the operation of the concatenated AND logic gates as a keypad lock system. (B) Current output of the concatenated AND logic gates at different input combinations (1 and 0 indicated the presence and absence of the corresponding input, respectively). Three different inputs were concurrently introduced in the sensing system, and the final electrochemical response was employed as the output signal. (C) Current change (current difference before and after last input) as the signal output of the concatenated AND logic gates at different input combinations. (D) Current outputs of the keypad lock at different permutations of three inputs (a, b, and c). (E) Reset cycles of the keypad lock by different input permutations.

inhibition of the soluble redox indicator toward the electrode surface (curve d). With the further incubation with dig-DNA3, a slight increase of R_{ct} could be observed (curve e). After DNA3 extension for the release of DNA1 by DNA polymerase, the modified electrode was finally converted into the DNA1-assembled electrode, which was witnessed with a drastic decrease of R_{ct} (curve f). The cyclic voltammetric characterizations toward the streamlined workflow of the biosensor could be in good accordance with the EIS results (Figure S10). Furthermore, the current changes related with each step (signal suppression for step 1 and signal enhancement for steps 2 and step 3) displayed the protein concentration-dependent response behaviors (Figure 4E).

Operation of the Concatenated AND Logic Gates as a Molecular Keypad Lock System. Inspired by the successive monitoring ability of the current streamlined workflow toward separate inputs of different biomolecules, a proof of concept for the operation of the concatenated AND logic gates as a new keypad lock security system was proposed and is schematically shown in Figure 5A. The immobilized duplex DNA scaffold was used as the initial state. The protein, DNA3, and polymerase were used as three consecutive inputs (inputs a, b, and c, respectively). The output event of one gate served as one of the input events for a downstream gate. For the first AND logic gate, the protein (input a) was bound with the duplex DNA scaffold (initial state) to form the protein-recognized electrode (electrochemical signal was suppressed). Then, the DNA3 (input b) was entered to interact with the protein-recognized electrode for the second AND logic gate, inducing the DNA1 sequence to be partially released for the evidently enhanced electrochemical signal response. The further introduction of DNA polymerase/dNTPs (input c)

https://doi.org/10.1021/acs.analchem.2c00800
Anal. Chem. 2022, 94, 8317−8326

triggered the third AND logic gate, and the completely released DNA1 contributed to the further enhanced electrochemical signal. After each AND logic operation, a simple rinsing of the electrode was sufficient to avoid the unwanted reactions or chemical accumulations.

We first studied the concatenated AND logic gates by concurrently introducing three different inputs, and the final electrochemical response was employed as the output signal (Figure 5B). The input was regarded as 1 when it was present and 0 if it was absent. The maximum current output was only observed in the situation of the (1,1,1) input state owing to the complete release of DNA1 from the initial duplex DNA scaffold. For other input combinations, the current outputs were comparable or lower than those of the initial state (duplex DNA scaffold-immobilized electrode) except the situation of (1,1,0). For the (1,1,0) situation, the electrode presented the status that the DNA1 was partially released from the duplex DNA probe by protein binding and DNA3-induced strand displacement. In this state, the current output was larger than that of the initial state of the electrode but far lower than that of the maximum current output. Using a self-settable current threshold value (dotted line), a current output evidently higher than the threshold value by the (1,1,1) input reported the "ON" state, and current outputs lower than the threshold value by other input situations indicated the "OFF" states of the concatenated AND logic gates. Despite the good discrimination between "ON" and "OFF" states, a relatively large current threshold value was needed that increased the possibility of the false output risk. To address this issue, the inputs were stepwise introduced, and the current responses before and after the last input were recorded. Then, the current change between them was used as the output signal for further evaluation (Figure 5C). A large current difference before and after the last input could be only observed for the input (1,1,1). Only very weak current difference was obtained for other input combinations, indicating a largely upgraded discrimination ability.

For a security keypad lock system, its true output signal should also depend on the correct order of the inputs. The order of the three inputs with the total six arrangments (abc, acb, bac, bca, cab, cba) was studied. It could be seen from Figure 5D that only one correct order of the three inputs (abc) could result in the maximum current readout owing to the complete release of DNA1 from the initial duplex DNA scaffold probe. This electrode status was considered as the true output signal ("ON" state), corresponding to the correct password (abc) to open the keypad lock. All other wrong orders of the three inputs could only induce the electrodes presenting protein binding (bac, bca, and cba) or protein binding and DNA3-induced partial release of DNA1 (acb and cab). These obtained electrodes generated much lower current readouts, which were considered as the false output signals ("OFF" state), indicating the failure to open the keypad lock. Again, a relatively large current threshold value should be used to indicate the "ON" or "OFF" states of the keypad lock system. To address it, the current changes corresponding to each input were obtained and are shown in Figure S11A. Only the correct order of the three inputs (abc) could simultaneously induce the evident current enhancements for both input 2 and 3. Other wrong orders of the three inputs might induce the current enhancement for the third input (for example, the inputs acb and cab) but not for the second input. Thus, based on the current changes induced by the second and third inputs, the success or failure to open the keypad lock could be effectively evaluated. To simplify the measurement step, the current outputs before and after the last input were measured and are displayed in Figure S11B. In this case, only the correct order of the input information (abc) could generate the obvious current responses for both measurements (before and after the last input). As for other wrong orders of the three inputs, the electrochemical responses for both measurements were evidently lower than those of the correct order. It thus provided a double-check means to indicate the success or failure to open the keypad lock. The developed keypad lock could also be reset from both "ON" and "OFF" states (Figure 5E). If the keypad lock occurred with the "ON" state by the correct password (input abc), the DNA1-only-immobilized electrode was produced. After its direct hybridization with DNA2, the duplex DNA scaffold-modified electrode was obtained, and the keypad lock system was returned to its initial state. For other wrong orders of the inputs, the keypad lock stayed in the "OFF" state, and the protein-recognized electrodes were always presented. With the further addition of the inputs b and c in sequence, the DNA1-immobilized electrodes could also be generated. Then, the keypad lock could return to its initial state after hybridization with the DNA2. After resetting of the keypad lock, the "ON" or "OFF" states could be reached again when the system was triggered by the input abc or other five permutations.

CONCLUSIONS

In summary, a flexible and universal DNA-based sensing platform was developed for multiple assay modes of protein and a keypad lock security system using an interface of only one duplex DNA scaffold. It could be harnessed for three different signal response behaviors (one signal-off and two signal-on modes) toward the sensitive and selective detection of the target protein. It could also be deployed as a streamlined electrochemical workflow for the consecutive monitoring of protein binding. Furthermore, it could be applied for the operation of an electrochemical keypad lock system. The current versatile duplex DNA scaffold-based sensing platform was simple in design and easy-to-operate but well-controllable in signal transduction and sensing performance, and it thus offered a new avenue for the development of high-performance biosensors or logic devices to be applied for molecular diagnosis or computing.

ASSOCIATED CONTENT

Supporting Information

The Supporting Information is available free of charge at https://pubs.acs.org/doi/10.1021/acs.analchem.2c00800.

DNA sequences; detection performance comparison; recovery experiments; electrode characterizations; control experiments; fluorescence characterizations; protein detection performance; biosensor fabrication process; and keypad lock (PDF)

AUTHOR INFORMATION

Corresponding Author

Shufeng Liu − *College of Chemistry and Chemical Engineering, Yantai University, Yantai 264005, China;* orcid.org/0000-0003-4063-4537; Email: sliu@ytu.edu.cn

https://doi.org/10.1021/acs.analchem.2c00800
Anal. Chem. 2022, 94, 8317−8326

Authors

Li Wang − *College of Chemistry and Chemical Engineering, Yantai University, Yantai 264005, China*

Xu Wang − *College of Chemistry and Molecular Engineering, Qingdao University of Science and Technology, Qingdao 266042, China*

Zhiqiang Chen − *College of Chemistry and Molecular Engineering, Qingdao University of Science and Technology, Qingdao 266042, China*

Complete contact information is available at: https://pubs.acs.org/10.1021/acs.analchem.2c00800

Notes

The authors declare no competing financial interest.

■ ACKNOWLEDGMENTS

This work was supported by the Natural Science Foundation of Shandong Province (JQ201704), the National Natural Science Foundation of China (21475072), and the Key Research and Development Program of Shandong Province of China (2016GSF201208).

■ REFERENCES

(1) Urdea, M.; Penny, L. A.; Olmsted, S. S.; Giovanni, M. Y.; Kaspar, P.; Shepherd, A.; Wilson, P.; Dahl, C. A.; Buchsbaum, S.; Moeller, G.; Burgess, D. C. H. *Nature* **2006**, *444*, 73−79.

(2) Fredriksson, S.; Gullberg, M.; Jarvius, J.; Olsson, C.; Pietras, K.; Gústafsdóttir, S. M.; Östman, A.; Landegren, U. *Nat. Biotechnol.* **2002**, *20*, 473−477.

(3) Yadav, S.; Kashaninejad, N.; Kamal, M.; Yamauchi, Y.; Nguyen, N. T.; Shiddiky, M. J. A. *Biosens. Bioelectron.* **2019**, *139*, No. 111315.

(4) Tighe, P. J.; Ryder, R. R.; Todd, I.; Fairclough, L. C. *Proteomics: Clin. Appl.* **2015**, *9*, 406−422.

(5) de la Rica, R.; Stevens, M. M. *Nat. Nanotechnol.* **2012**, *7*, 821−824.

(6) Sinkala, E.; Sollier-Christen, E.; Renier, C.; Rosàs-Canyelles, E.; Che, J.; Heirich, K.; Duncombe, T. A.; Vlassakis, J.; Yamauchi, K. A.; Huang, H.; Jeffrey, S. S.; Herr, A. E. *Nat. Commun.* **2017**, *8*, No. 14622.

(7) Cohen, L.; Walt, D. R. *Chem. Rev.* **2019**, *119*, 293−321.

(8) Borrebaeck, C. A. K. *Nat. Rev. Cancer* **2017**, *17*, 199−204.

(9) Mariani, S.; Robbiano, V.; Strambini, L. M.; Debrassi, A.; Egri, G.; Dähne, L.; Barillaro, G. *Nat. Commun.* **2018**, *9*, No. 5256.

(10) Mocenigo, M.; Porchetta, A.; Rossetti, M.; Brass, E.; Tonini, L.; Puzzi, L.; Tagliabue, E.; Triulzi, T.; Marini, B.; Ricci, F.; Ippodrino, R. *ACS Sens.* **2020**, *5*, 3109−3115.

(11) Zong, C.; Wu, J.; Liu, M.; Yan, F.; Ju, H. *Chem. Sci.* **2015**, *6*, 2602−2607.

(12) Labib, M.; Sargent, E. H.; Kelley, S. O. *Chem. Rev.* **2016**, *116*, 9001−9090.

(13) Drummond, T. G.; Hill, M. G.; Barton, J. K. *Nat. Biotechnol.* **2003**, *21*, 1192−1199.

(14) Das, J.; Kelley, S. O. *Anal. Chem.* **2011**, *83*, 1167−1172.

(15) Grewal, Y. S.; Shiddiky, M. J. A.; Gray, S. A.; Weigel, K. M.; Cangelosi, G. A.; Trau, M. *Chem. Commun.* **2013**, *49*, 1551−1553.

(16) Farjami, E.; Clima, L.; Gothelf, K.; Ferapontova, E. E. *Anal. Chem.* **2011**, *83*, 1594−1602.

(17) Schoukroun-Barnes, L. R.; Macazo, F. C.; Gutierrez, B.; Lottermoser, J.; Liu, J.; White, R. J. *Annu. Rev. Anal. Chem.* **2016**, *9*, 163−181.

(18) Li, D.; Song, S.; Fan, C. *Acc. Chem. Res.* **2010**, *43*, 631−641.

(19) Vallée-Bélisle, A.; Ricci, F.; Uzawa, T.; Xia, F.; Plaxco, K. W. *J. Am. Chem. Soc.* **2012**, *134*, 15197−15200.

(20) Das, J.; Gomis, S.; Chen, J. B.; Yousefi, H.; Ahmed, S.; Mahmud, A.; Zhou, W.; Sargent, E. H.; Kelley, S. O. *Nat. Chem.* **2021**, *13*, 428−434.

(21) Cash, K. J.; Ricci, F.; Plaxco, K. W. *J. Am. Chem. Soc.* **2009**, *131*, 6955−6957.

(22) Somasundaram, S.; Easley, C. J. *J. Am. Chem. Soc.* **2019**, *141*, 11721−11726.

(23) Mahshid, S. S.; Camiré, S.; Ricci, F.; Vallée-Bélisle, A. *J. Am. Chem. Soc.* **2015**, *137*, 15596−15599.

(24) Mahshid, S. S.; Vallée-Bélisle, A.; Kelley, S. O. *Anal. Chem.* **2017**, *89*, 9751−9757.

(25) Rossetti, M.; Brannetti, S.; Mocenigo, M.; Marini, B.; Ippodrino, R.; Porchetta, A. *Angew. Chem., Int. Ed.* **2020**, *59*, 14973−14978.

(26) Bezerra, A. B.; Kurian, A. S. N.; Easley, C. J. *Anal. Chem.* **2021**, *93*, 198−214.

(27) Zhang, H.; Li, F.; Dever, B.; Wang, C.; Li, X. F.; Le, X. C. *Angew. Chem., Int. Ed.* **2013**, *52*, 10698−10705.

(28) Hu, J.; Yu, Y.; Brooks, J. C.; Godwin, L. A.; Somasundaram, S.; Torabinejad, F.; Kim, J.; Shannon, C.; Easley, C. J. *J. Am. Chem. Soc.* **2014**, *136*, 8467−8474.

(29) Traynor, S. M.; Wang, G. A.; Pandey, R.; Li, F.; Soleymani, L. *Angew. Chem., Int. Ed.* **2020**, *59*, 22617−22622.

(30) Tang, Y.; Wang, Z.; Yang, X.; Chen, J.; Liu, L.; Zhao, W.; Le, X. C.; Li, F. *Chem. Sci.* **2015**, *6*, 5729−5733.

(31) Du, Y.; Han, X.; Wang, C.; Li, Y.; Li, B.; Duan, H. *ACS Sens.* **2018**, *3*, 54−58.

(32) Chen, J.; Zhou, S.; Wen, J. *Angew. Chem.* **2015**, *127*, 456−460.

(33) Li, H.; Hong, W.; Dong, S.; Liu, Y.; Wang, E. *ACS Nano* **2014**, *8*, 2796−2803.

(34) Bard, A. J.; Faulkner, L. R. *Electrochemical Methods: Fundamentals and Applications*, 2nd ed.; Wiley: New York, 2001.

(35) Fan, C.; Plaxco, K. W.; Heeger, A. J. *Proc. Natl. Acad. Sci. U.S.A.* **2003**, *100*, 9134−9137.

(36) Zuo, X.; Song, S.; Zhang, J.; Pan, D.; Wang, L.; Fan, C. *J. Am. Chem. Soc.* **2007**, *129*, 1042−1043.

(37) Steel, A. B.; Herne, T. M.; Tarlov, M. J. *Anal. Chem.* **1998**, *70*, 4670−4677.